Slide Material Test - Test Report

Authors: C. Darve, Y. Huang, J.F. Legner, T. Nicol, T. Wokas, G. Zielbauer

Abstract

Fermilab will supply 32 cryostats for the LHC IR inner triplet quadrupole magnets. The cryostat system needs to support the cold mass, which houses the quadrupole magnet. In order to allow the thermal contraction displacements between the 1.9 K cold mass and the 300 K cryostat vacuum vessel, a sliding system made out of bushings was designed and integrated to the cryostat design. The chosen material will permit the 20,000 lbs cold mass to slide with respect to the vacuum vessel. The material needs to be radiation resistant and to work at cryogenic temperatures.

A slide material test setup was designed and built at Fermilab. The goal of the test was to measure the friction coefficient of several materials at cryogenic temperature and under vacuum. Ten different materials were tested in order to simulate the pin (rod) and bushing system.

1 INTRODUCTION

In the framework of the US-LHC interaction region design studies for the inner triplet magnet cryostat, we investigated the friction coefficient of sliding materials.
The LHC IR cryostat serves to support the superconducting magnet accurately and reliably within the vacuum vessel, to provide all required cryogenic piping and to insulate the cold mass from heat radiated and conducted from the environment. The cryostat provides the alignment of the cold mass inside of the cryostat. The cold mass shrinks during the cold down due to the materials thermal contraction differences, hence the supporting system must be able to slide in order to minimize the stresses and keep the alignment.

A model of the sliding system was developed at Fermilab and tested in the Technical Division Engineering Laboratory. The sliding system under investigation was composed of the bushing and the pins. The purpose of the test was to measure the friction coefficient of several material combinations. This test simulates the thermo-mechanical behavior of the LHC IR quadrupole pin/bushing system. Hence, this test permits us to qualify the bushing material to be used for the LHC.

2 DESCRIPTION OF THE LHC SUPPORT RING SYSTEM

The cryostat permits us to assure the supporting function between the cold mass and the cryostat vacuum vessel. Two composite spiders support each 7-m long magnet. Figure 1 shows the parts, which assure the supporting function. The slide material is located inside the bushing attached to the G11 spider. It slides on the pin which is attached rigidly to the cold mass. Figure 2 illustrates the view of the final LHC ring support system.

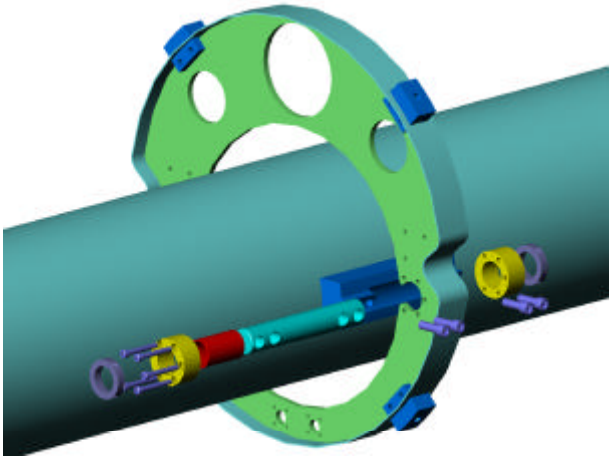

Figure 1. Schematic of the support ring to cold mass connection

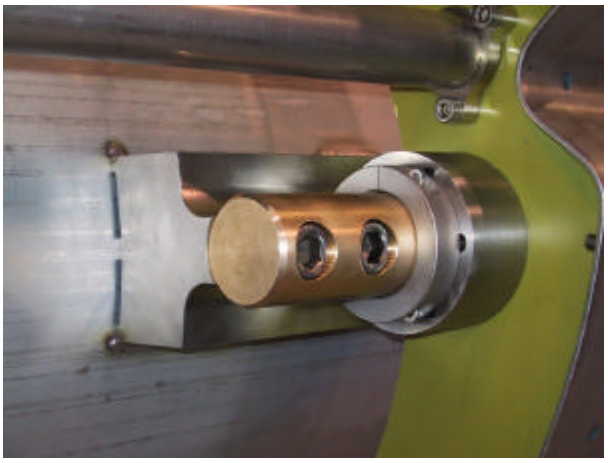

Figure 2. View of the support ring to cold mass connection

3 MODELISATION OF THE SLIDE MATERIAL TEST

3.1 Principle of the measurement

In order to measure the friction coefficient of the LHC IR quadrupole pin/bushing system, we can reduce the analysis to the schematic presented in figure 3 a). Several materials can be defined as A and B, the bushing and the pin, respectively. Two perpendicular loads F1 and F2 are applied to the pin and the bushing respectively. F1 simulates the friction force during cool down. F2 simulates the weight of the LHC IR quadrupole.

The display of all parts should characterize the connection between the LHC IR cold mass pin and the support spider bushing. The cold mass supporting system can be simulated by the use of 3 sub-assemblies (Figure 3). The load F2 is only applied on the central bushing A. The two outboard bushings simulate the bushings, which are housed in the support spider, therefore they are fixed in our setup. The friction coefficient, *f*, at their interface can be expressed by:

$$f = F1/F2 \qquad (1)$$

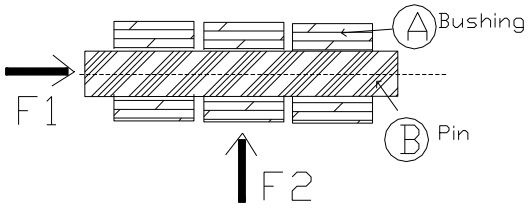

Figure 3: Measurement of the friction coefficient

The principle of the measurement is to apply a fixed load F2 and to measure the force F1 needed to move the pin. The friction coefficient, *f*, is calculated out of these forces. The load F2 is increased gradually and a similar approach are observed for each step.

These measurements are first performed at room temperature. In the next stage, we evacuate the cryostat down to a vacuum of approximately $7x10^{-2}$ mbar and finally we cool the system down to LN_2 temperature. The measurements are repeated for both vacuum and cold temperature conditions.

3.2 Equivalent of the LHC IRQ parameters

The cold mass weight is transmitted to two supports spider via four pins. A model of the interface between the pin and the bushing was developed and the parts dimensions were estimated. The full-scaled LHC IR supporting system was scaled down to match our test setup. We considered a 25.4 mm outer diameter pin instead of 50 mm in the LHC case. We calculated the final tolerance of the pin and bushing to be machined and finished by taking into account the thermal contraction of the materials.

3.3 Contact surface

The contact surface will be used to calculate the thermal parameters of the system. Hence we would need to know the contact area between the pin and the bushing. The following paragraph introduces this consideration. If we consider a cylinder and a cylindrical cavity with parallel axis, then we can determine the contact surface and the maximum stress. The wide of the contact surface was estimated for material A and B, representative of the bushing and the pin. μ_A and μ_B are the Poisson coefficients, E_A and E_B are the Young's modulus. P is the pressure applied to the pin (F1/S in our case) and L is the length of the contact between the pin and the bushing, R_A and R_B are the inner radius of the bushing and the outer radius of the pin, respectively. The estimation of the width and length of the bushing permit us to determine the force applied and to define the heat load transferred from one system to the other.

$$width = 2 \cdot 1.128 \sqrt{\frac{P}{L}\left[\left(\frac{\left(1-m_A{}^2\right)}{E_A}\right)+\left(\frac{\left(1-m_B{}^2\right)}{E_B}\right)\right]\left(\frac{R_A \cdot R_B}{\left(R_A - R_B\right)}\right)} \qquad (2)$$

Ex: Let's consider a stainless steel pin and a HDPE bushing with an applied pressure of 1,000 psi. If the length of the contact is 38 mm and the radius of the pin and bushing are 17.5 mm and 18 mm, respectively, then the contact wide is 0.6 mm.

4 TEST SETUP DESIGN

4.1 Assembly and cryogenic set-up

In order to simulate the LHC IR conditions, the test was performed at cryogenic temperatures and in vacuum. The thermal contractions are important in the temperature range 300 K to 77 K, hence we chose liquid nitrogen to run the test at cold temperature.

Figure 4 illustrates the set-up. Adapters permit us to integrate the bushings in the system as well as to provide the cooling of the system. A pump permits us to evacuate the cryostat down to approximately $7x10^{-2}$ mbar. Liquid nitrogen circuit provides a quasi-uniform temperature distribution to the outer surface of the bushings due to a cooling tube brazed to the adapters. A PC recorded loads, pressure and temperature measurements.

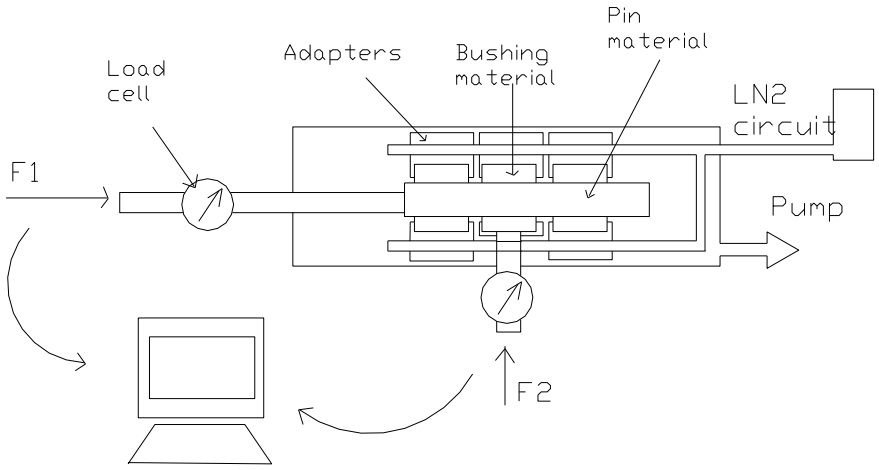

Figure 4: Test set-up

The assembly was installed in the Engineering Lab. Figure 5 shows the assembly drawing. The load cells, items 35, transmit F1 and F2, by means of two hydraulic cylinders, item 34. Item 13 is the pin, 14 are the bushings. Item 16 are adapters for the three sub-assemblies (bushing/pin). Item 12 and 15 are the blocks that house the adapters, they are cooled at LN_2 temperature. Composite plates (G10), item 9, insulate the system.

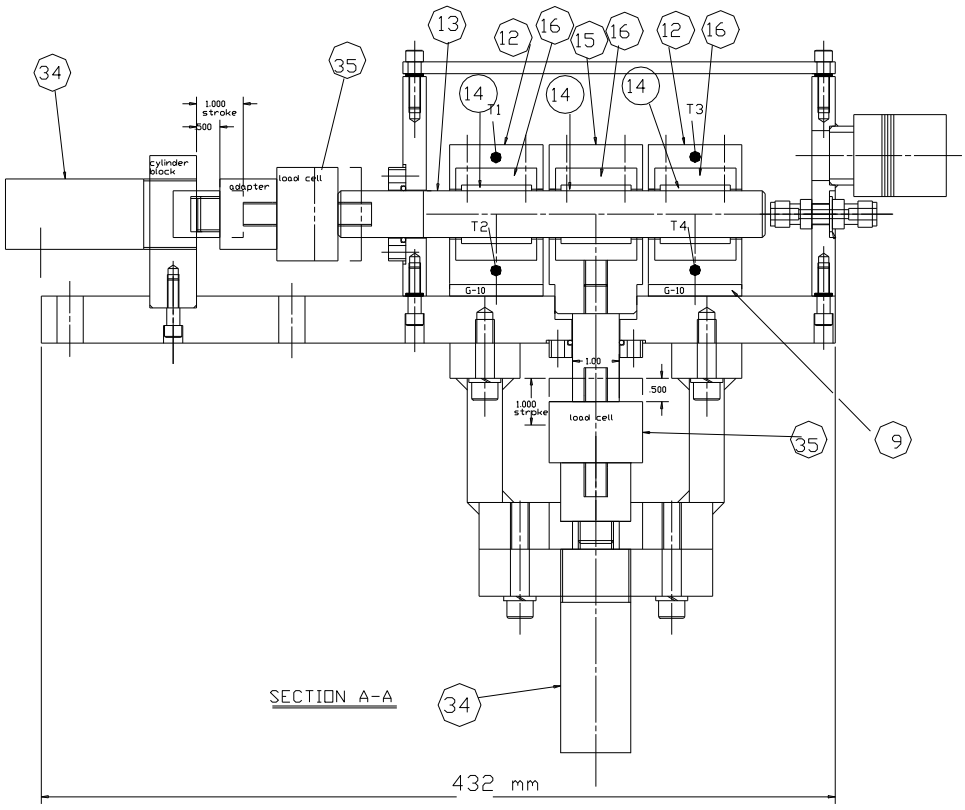

Figure 5: Full assembly located in the cryostat

4.2 Instrumentation

Load cells, temperature sensors, mass-flow meter and pressure gages are the main instrumentation used for this test run. The two load-cells permit to measure the force F1 and F2 defined in the previous section.
For the loads of interest and for the friction coefficient found in the literature, of about 0.4, we can estimate that the load F1 should be in the range of 500 lbs. Therefore we can consider a larger range for the test, the selected calibrated load cells will cover the ranges:

F1 = -/+ 1,000 lbs (453 kg)
F2 = -/+ 2,500 lbs (1,133 kg)

The instrumentation list and their characteristics are summarized in table 4. Four platinum temperature sensors (T1, T2, T3, T4) are mounted with stycast in holes machined in the adapters (see figure 5). The load cells are calibrated in compression.

Hydraulic cylinders provide the pressure, which is measured by the load cells. The pressure is increased gradually using hydraulic pumps connecting the cylinders. These hydraulic pump can have a resolution as low as 25 psi for applied pressure lower than 100 psi. The resolution is about 4 psi for larger pressures. Pressure gages were interchanged depending on the pressure range of concern. The error of the measurement is estimated to 10 %.

Table 1: Characteristics of the instrumentation

Instrumentation	**Excitation**	**Output**	**Range**	**Use/ qty**
Load cell	10 V dc	2 mV / V +/-25%.	0-1,000 lbs 0-2,500 lbs	Measure force / 2
Cylinder hydraulic	10,000 psi	5 ton	5 ton	Provide the force / 2
Hydraulic pump	Manual		0-3,000 psi	Measure pressure for the cyl. / 1
Platinum resistance	100 μA	2 mV	2 mV	Measure Temperature / 4
Pressure transducer	-/+ 15 V		10^{3}-10^{-2} mbar	Vacuum measurement / 1
Mass flow-meter	5 V		0-50 g/s	Measure Nitrogen massflow / 1

4.3 Materials under investigation

Materials have been selected based on their physical, thermal and mechanical properties. The chosen material must be radiation resistant and usable at cryogenic temperature as low as 2 K [1]. The friction coefficient of these materials are rarely given by the literature. The different materials tested for the pin and the bushing are listed in table 2. Aerolex lubricant was used to coat the bronze pin.

Table 2: Properties of selected materials

Material A - Bushing			
	Friction coeff. *	**Young modulus E**	**Thermal expansion**
Unit		**GPa**	**10^{-6} K^{-1}**
Vespel	0.2-0.42	3.2	30-60
Rulon LR	0.15-0.25	$13.8.10^{-3}$	82
Teflon	0.04-0.2	0.3-0.8	100-160
DU	0.02-0.2	0.3	30
Al, bronze	0.1-0.3	80-110	16.9
Graphite	0.1	2-17	0.6-4.3
Graphite plugged Bronze	0.1	2-17	0.6-4.3

* As found in the literature

Material B - Rod			
Stainless Steel - 304	0.1-1.1	190-210	18.0
Bronze	0.2	80-110	16.9
Bronze w/ aerolex coating		80-110	17

Other material A under investigation - not reported here			
Ultem 1000		2.9	56
Lead	0.9	14	29
Torlon		4.5-6.8	25-31
HDPE	0.29	0.5-1.2	100-200

5 RESULTS

5.1 Measurements

Materials available for the bushing and pin are combined for the test. The friction coefficient was measured for three cases: ambient, vacuum and cryogenics temperatures.

The principle of the measurement is to apply a fixed load F2, and to acquire data (loads, temperatures) for at least 100 points per fixed load F2. The friction coefficient is calculated out of the average data.

The cool-down lasts about 2 hours to reach ~ 100 K. Figure 6 shows the results for a graphite bushing. For the measurements at cold temperature the vacuum was 7.10^{-2} mbar and the temperature 100 K. We measured a friction coefficient equal to 0.27 for the bronze pin. The figure shows that the friction coefficient decreases when the pressure increases. The stabilization of this evolution exists after 1,000 psi.

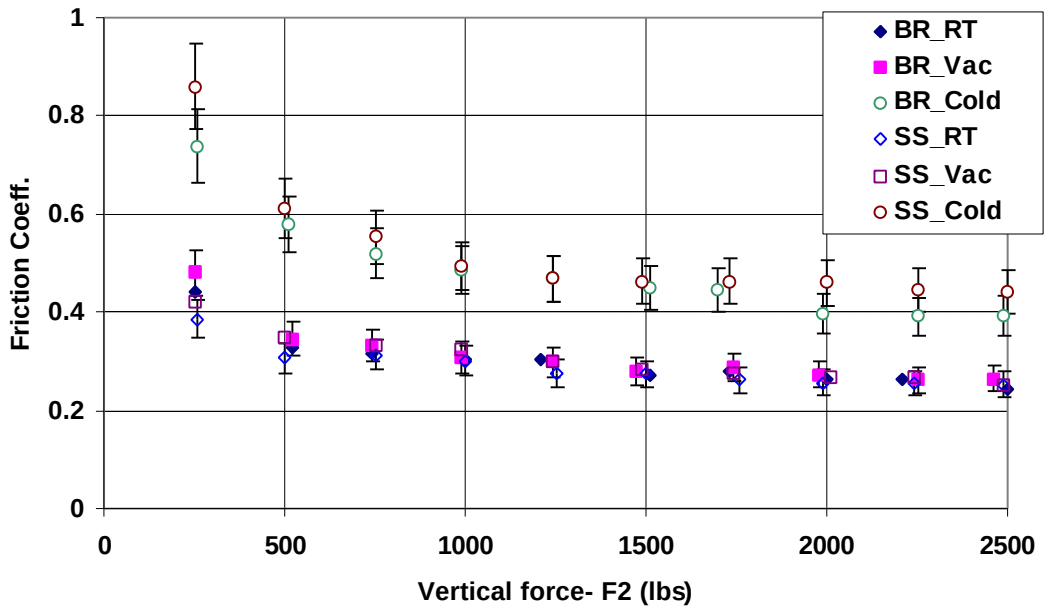

Figure 6: Friction coefficient vs. the force F2, for a graphite bushing with both stainless-steel and bronze rods.

Figure 7 shows the results for a Bronze/DU bushing. For cold temperature measurements the vacuum was $7x10^{-2}$ mbar and the temperature 100 K. The friction coefficient measured was 0.04 using a bronze pin.

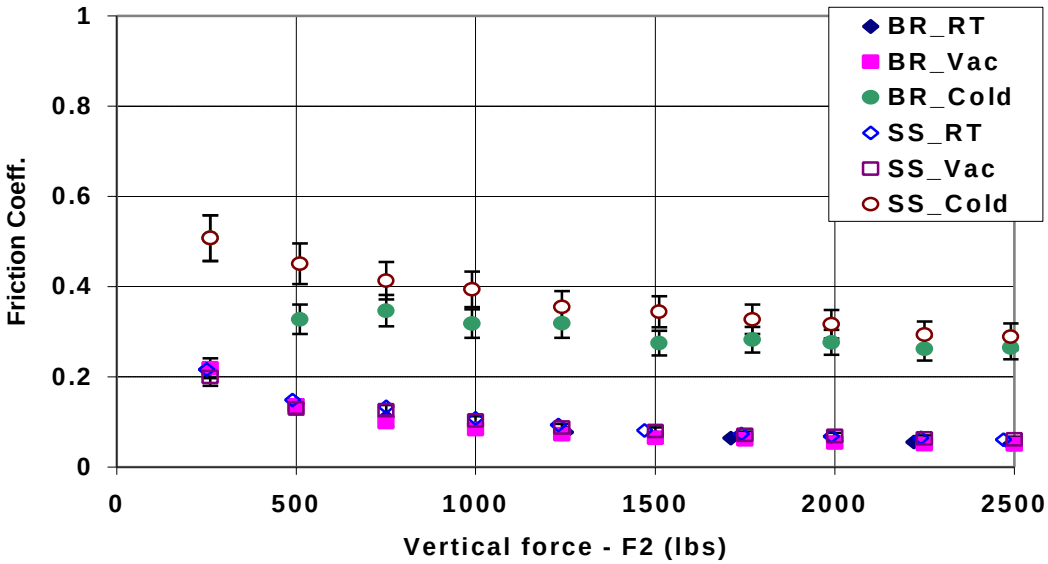

Figure 7: Friction coefficient vs. the force F2, for a DU bushing with both stainless-steel and bronze rods.

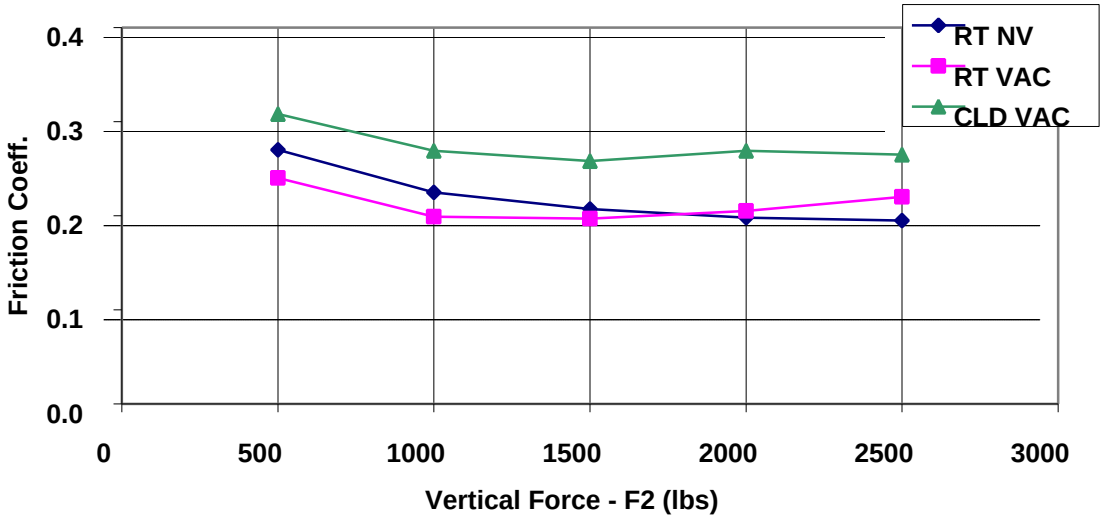

Figure 8: Friction coefficient vs. the force F2, for a DU bushing and bronze rod.

As both figures 6 and 7 show, the friction coefficient becomes stable with P2 larger than 1,000 psi. This observation can be due to the contact surface, which remains the same for high pressure. The stabilization is observed for higher pressure for material with a high Young's modulus, E. Table 5, lists all the performances of the other combination tested. The friction coefficients are determined for pressure equivalent to 2,000 psi.

Table 5: Results table

	Mat #	Vespel	Rulon	Teflon	DU	Bronze-Al	Graphite	Graph plugged Br
Room Temp.	**SS**	0.292	0.137		0.089	0.371	0.256	0.364
	Bronze		0.139	0.198	0.072		0.265	0.285
	Bronze coated	0.221	0.128					
Vacuum	**SS**	0.343	0.140		0.081	0.474	0.269	0.417
	Bronze		0.140	0.205	0.067		0.273	0.296
	Bronze coated	0.278	0.132					0.051
Cold & vac	**SS**	0.600	0.302		0.355		0.460	0.574
	Bronze		0.300	0.269	0.340		0.397	0.369
	Bronze coated	0.591	0.210					

The measurements show that vacuum conditions ($7x10^{-2}$ mbar) do not degrade the friction coefficient in a significant way. However the cold temperature is an important parameter for the change in friction property of the materials.

The use of the bronze pin instead of the stainless steel pin represents about 11 % of improvement of the friction coefficient at cryogenic temperatures.

The DU bushing presents some characteristics, which are very favorable for the friction, while used with a bronze pin. By comparison the use of DU at room temperature shows an improvement of 80 % of the performance compared to the graphite bushing.

More information about this test is available at http://tspc01.fnal.gov/darve/Smt/smt.html.

5.2 Radiation damage

Radiation is an issue for the LHC operations. The radiation at the proximity of the cold mass was calculated equal to 9.5×10^4 Gy over a 7-year lifetime at nominal luminosity (see appendix). The DU-bronze although composed of Teflon would still be marginally acceptable in this location. We are investigating methods to passively shield the bushings from radiation. In addition we are pursuing the use of a facility to irradiate sample DU bushings for subsequent retesting.

6 CONCLUSION

The slide material test permitted us to qualify different materials regarding their friction coefficient. The different materials friction coefficients were measured at ambient, vacuum and cold temperature conditions. The low vacuum conditions do not contribute to change the sliding function of the considered system significantly, whereas the cold temperature conditions do. Degradation of the sliding function up to 80 % was measured at cold temperature.

The supporting system of the LHC IR cold mass will be based on the choice of DU bushing and bronze pin. The friction coefficient of this combination is approximately 0.3 in vacuum and at cryogenic temperatures.

Reference:

[1] CERN 96-05, "Results of Radiation Tests at Cryogenic Temperature on Some Selected Organic Materials for the LHC", H. Schonbacher, B. Szeless , M. Tavet, K. Humer and H.W. Weber.

Appendix

RESULTS OF RADIATION TESTS AT CRYOGENIC TEMPERATURE ON SOME SELECTED ORGANIC MATERIALS FOR THE LHC

H. Schönbacher, B. Szeless and M. Tavlet
CERN, 1211 Geneva 23, Switzerland

and

K. Humer and H.W. Weber
Atominstitut der Österreichischen Universitäten, 1020 Vienna, Austria

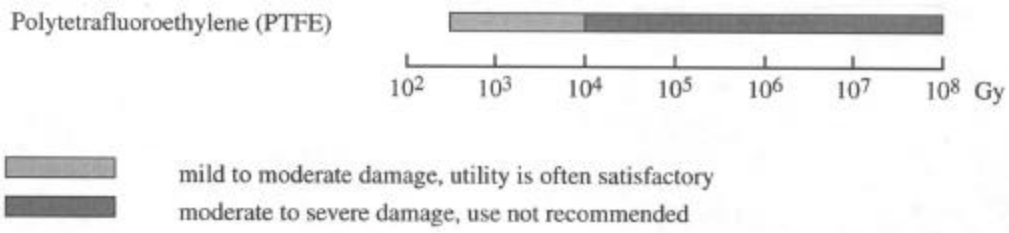

mild to moderate damage, utility is often satisfactory

moderate to severe damage, use not recommended

These appreciations can only serve as a general guideline; environmental conditions such as temperature, humidity and dose rate, as well as additives influence the radiation behaviour of materials.

Fibre reinforced composites based on these resins can be at least one order of magnitude better.

Subject: Radiation numbers for cryostat
Date: Tue, 22 Aug 2000 11:38:16 -0500 (CDT)
From: Nikolai Mokhov <mokhov@fnal.gov>

Azimuthal variation of dose at such radii is much less than that for the coils. From our spring's results I found that the peak doses Dmax are only a factor of 1.5 (a factor of 2 at a couple of occasions) higher than the azimuthally averaged doses D. For the baseline luminosity and corresponding arithmetic (luminosity reduction over a store, 180 days per year etc, see my message of 02/12/99) with the above factor of 1.5, we get

	D (kGy/yr)	Dmax (kGy/yr)
24.07m from IP, 0.25m radius	1.5	2.3
28.25m from IP, 0.25m radius	3.5	5.3
33.26m from IP, 0.208m radius	5	7.5
37.80m from IP, 0.208m radius	6.5	9.8
42.34m from IP, 0.208m radius	9	13.5
48.34m from IP, 0.25m radius	5	7.5
52.53m from IP, 0.25m radius	5	7.5

For the above locations, I have also generated radial distributions of the azimuthally averaged dose ($2 < r < 25$ cm). Let me know if you need those plots.

Cheers,
Nikolai